Imaging Science in Dentistry 2023; 53: 247-56
https://doi.org/10.5624/isd.20220223

Importance of 3-dimensional imaging in the early diagnosis of chondroblastic osteosarcoma

Laura Althea Cuschieri[1], Rebecca Schembri-Higgans[1], Nicholas Bezzina[1], Alexandra Betts[1], Arthur Rodriguez Gonzalez Cortes[1,*]

[1]*Department of Dental Surgery, Faculty of Dental Surgery, University of Malta, Msida, Malta*

ABSTRACT

The aim of this report is to present a case of chondroblastic osteosarcoma located in the right maxillary premolar region of a 17-year-old female patient. The initial clinical presentation and 2-dimensional (2D) radiographic methods proved inadequate for a definitive diagnosis. However, a cone-beam computed tomography scan revealed a hyperdense, heterogeneous lesion in the right maxillary premolar region, exhibiting a characteristic "sun-ray" appearance. To assess soft tissue involvement, a medical computed tomography scan was subsequently conducted. A positron emission tomography scan detected no metastasis or indications of secondary tumors. T1- and T2-weighted magnetic resonance imaging showed signal heterogeneity within the lesion, including areas of low signal intensity at the periphery. Histological examination conducted after an incisional biopsy confirmed the diagnosis of high-grade chondroblastic osteosarcoma. The patient was then referred to an oncology department for chemotherapy before surgery. In conclusion, these findings suggest that early diagnosis using 3-dimensional imaging can detect chondroblastic osteosarcoma in its early stages, such as before metastasis occurs, thereby improving the patient's prognosis. ***(Imaging Sci Dent 2023; 53: 247-56)***

KEY WORDS: Osteosarcoma; Cone-Beam Computed Tomography; Diagnostic Imaging: Radiography

Primary bone tumors presenting in the jaws are uncommon and are usually classified as being either odontogenic, composed of tooth-related/forming structures, or non-odontogenic.[1,2] Odontogenic tumors tend to exhibit characteristic radiographic features, usually associated with their proximity to specific teeth, which simplifies the diagnostic process.[2] An early diagnosis is crucial to avoid the necessity for aggressive invasive treatments, particularly for malignant jaw tumors that may exhibit rapid growth and metastasis. The radiographic appearance of the tumor depends on its stage; in the early stages, the size and boundaries of the lesion may be indistinct and challenging to identify.[3] The use of conventional 2-dimensional (2D) radiographs for the early diagnosis of tumors, as the presentation can vary from radiolucent to radiopaque, with or without an expansion of the periodontal ligament, none of which are pathognomonic.[1-4]

Osteosarcoma is the most common primary malignant bone tumor, excluding hematological malignancies.[5] Osteosarcomas are rare non-odontogenic tumors of the jaws and account for 6-7% of all skeletal osteosarcomas.[6] Typically, osteosarcomas are discovered in the third decade of life, with a slightly higher incidence in males.[7,8] They arise most frequently in the mandible as a firm swelling in the affected area.[9,10] Pain, paresthesia, a sudden increase in tooth mobility, and nasal obstruction are all area-dependent clinical features.[11] Osteosarcomas can develop in the context of pre-existing conditions, including hereditary retinoblastoma, fibrous dysplasia, a history of trauma, Paget's disease of bone, hereditary multiple osteochondromas, Li-Fraumeni syndrome, Rothmund-Thomson syndrome, chronic osteomyelitis, and osteogenesis imperfecta.[2,4,11] Osteosarcomas are classified into 3 types by their site of origin: 1) conventional type, 2) juxtacortical type, and 3) extraskeletal type. There are also 3 main histological subtypes based on whether they are predominantly composed of cartilage (chondroblastic), malignant bone and osteoid (osteoblastic),

Received September 26, 2022; Revised May 30, 2023; Accepted June 15, 2023
Published online August 2, 2023
*Correspondence to : Prof. Arthur Rodriguez Gonzalez Cortes
Department of Dental Surgery, Faculty of Dental Surgery, University of Malta, Block A, Level 0, Mater Dei Hospital, Msida MSD 2080, Malta
Tel) 356-9972-9634, E-mail) arthur.nogueira@um.edu.mt

Imaging Science in Dentistry · pISSN 2233-7822 eISSN 2233-7830

or spindle cells (fibroblastic).[2,5,10]

Osteosarcomas can display a variety of radiographic features, which can range from osteogenic to mixed, and even osteolytic patterns. Numerous studies have characterized the tumor by its radiopaque "sun-ray appearance," a result of irregular bone spicules developing outwardly and perpendicular to the lesion's surface once the tumor invades the periosteum.[5] Even though this feature is considered pathognomonic,[12] not all lesions have this particular presentation. Several studies have also described the tumor as having poorly defined margins, mixed radiolucencies, or in more advanced cases, a "moth-eaten" appearance.[2,13] The non-specific nature of these radiographic presentations can make diagnosis using conventional 2D radiographs particularly challenging, especially in the early stages of tumor formation. This can potentially lead to false negative results. Therefore, 3-dimensional (3D) imaging modalities, such as computed tomography (CT) and magnetic resonance imaging (MRI), are often necessary. These tools not only support the diagnosis, but also provide an accurate assessment of the tumor's size and stage, and help determine the involvement of soft and hard tissues.[5]

The pathologist's diagnosis is considered the gold standard for treatment planning and management.[14] However, early diagnosis of malignant tumors is often delayed due to their diverse clinical characteristics.[15] One study observed a shift in diagnosis from either an inflammatory or benign lesion to a malignant tumor in 30% of patients. This change occurred after a CT examination was performed following panoramic radiography, prior to histological analysis. For this 30%, the panoramic radiographs did not display the typical malignant pattern, particularly for tumors located in the maxilla.[15] Conventional intra- and extra-oral radiographs have limitations, including distortions, superimposition of anatomical structures, and magnification.[16,17] CT has been identified as the gold standard for diagnosing and treating intraosseous bone lesions, as it provides a comprehensive visualization of the lesion's size without superimpositions, using high-resolution imaging.[17] However, CT does expose the patient to high levels of radiation. Cone-beam computed tomography (CBCT) is considered a superior alternative for dental and maxillofacial regions due to its lower radiation dose and shorter imaging time. Yet, its low contrast resolution makes detecting soft tissue more challenging, and it is deemed insufficient for identifying soft tissue involvement.[18-21] Recent studies have sought to develop methods for early diagnosis of osseous lesions using deep learning-based diagnosis and/or pixel value utilization.[22-24]

Despite the existing evidence, there is limited knowledge about the early diagnosis of osteosarcoma using 3D imaging, particularly in cases where 2D images have failed to confirm a diagnosis. Therefore, the purpose of this article is to discuss a rare instance of chondroblastic osteosarcoma. In this case, 2D imaging techniques were inadequate for making a radiographic diagnosis, which was subsequently determined through CBCT analysis.

Case Report

A 17-year-old female presented at a private dental clinic, expressing concerns about swelling and discomfort in the upper right quadrant of her mouth that had persisted for

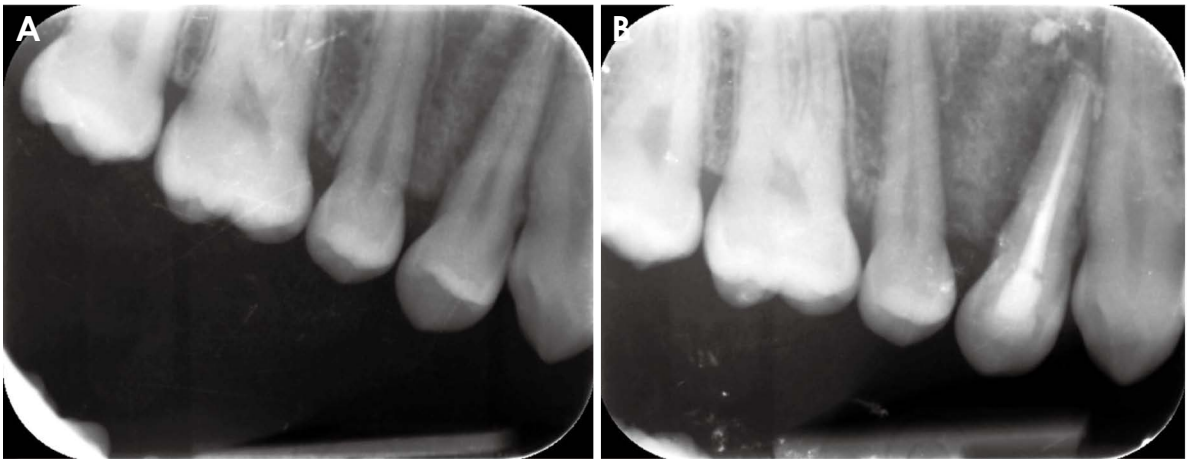

Fig. 1. Periapical radiographs of the upper right quadrant. A. A radiograph taken following the initial examination reveals a radiopaque image in the alveolar bone situated between the first and second premolars. B. A periapical radiograph, captured a few weeks post-completion of the root canal treatment on the maxillary right first premolar, displays a displacement of the first premolar and an enlarged, heterogeneous hyperdense area with indistinct boundaries located between the premolars.

Fig. 2. An intra-oral photograph, taken after the extraction of the first premolar, displays a nodular, ulcerated lesion with raised edges, partially covering the second premolar.

several weeks. The swelling was clinically observed around the apex of the maxillary right first premolar, as she reported. She did not report any associated symptoms such as numbness, fever, weight loss, difficulty breathing, or swelling in other areas. Her medical history did not contribute to her current condition. She does not smoke and maintains satisfactory oral hygiene.

On extraoral examination, a minor swelling was noticed beneath the nasolabial fold in the upper right quadrant. The lymph nodes in the head and neck region were not detectable through palpation. During the intraoral examination, the maxillary right first premolar appeared to be in good condition with no visible signs of decay. The distinct swelling was limited to the upper right premolar area, exhibiting

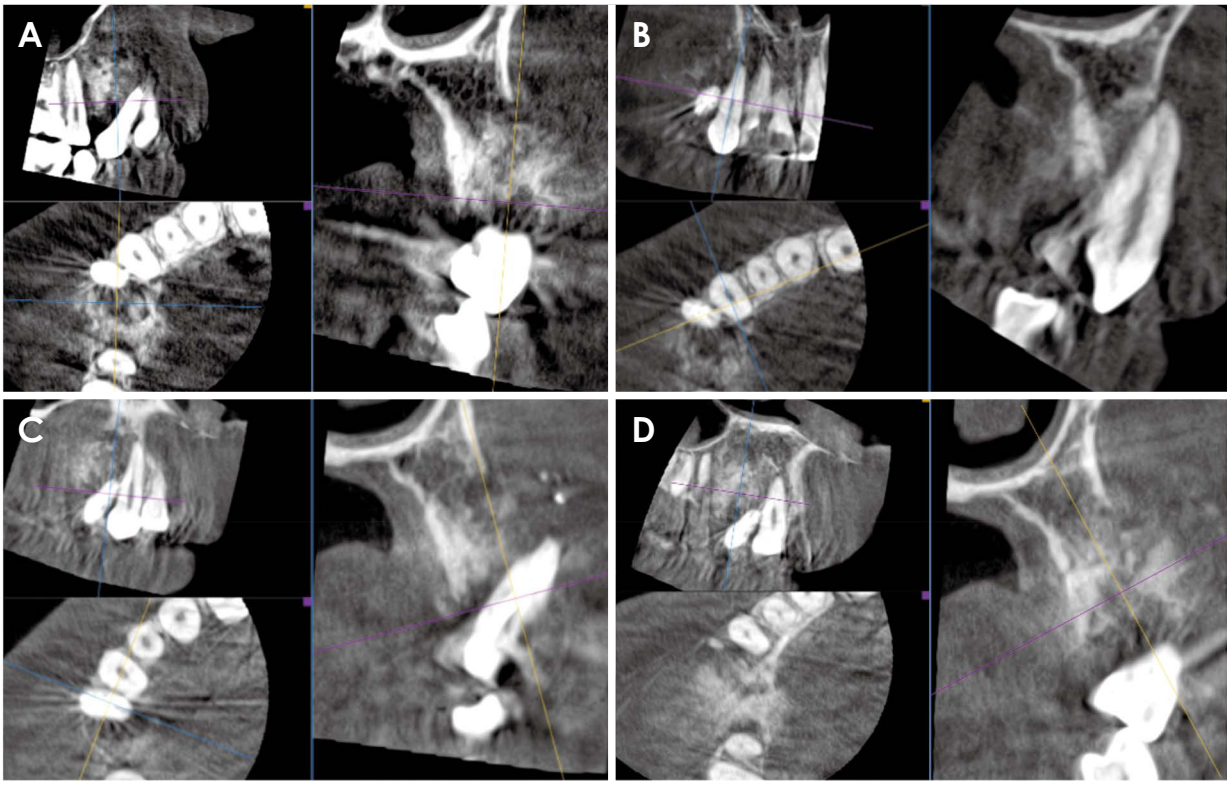

Fig. 3. Multiplanar reconstruction of the lesion, derived from 3-dimensional cone-beam computed tomographic images. A. Cross-sectional images enhanced by software contrast. Top left: Sagittal view of the second premolar site showing a mesial hypodense area of bone resorption and a distal heterogeneous hyperdense area of periosteal reaction; bottom-left: axial view showing buccal and palatal extensions of the lesion; right side: coronal view showing loss of the buccal bone plate and periosteal reaction, which exhibits a sun-ray appearance beneath a small hypodense area. This area is associated moth-eaten resorption of the buccal plate. B. Cross-sectional images of the maxillary right canine. Top left: Coronal oblique view showing hypodense areas of bone resorption at the distal aspect of the canine root; Bottom left: axial view of the canine site; right side: parasagittal view showing buccal displacement and an increased density of the alveolar bone, including palatal periosteal reaction. C. Cross-sectional images of the maxillary right first premolar. Top left: Oblique view showing a hypodense area suggestive of moth-eaten bone resorption apically to the first premolar and distal to the canine apex, with a distal hyperdense area suggestive of periosteal reaction; bottom left: axial view showing the hypodense area of the lesion distal to the first premolar; right side: parasagittal view showing buccal displacement of the first premolar and larger apical areas of moth-eaten resorption at the buccal aspect of the alveolar ridge. Note the hyperdense images, which suggest the presence of extruded endodontic material. D. Low-contrast cross-sectional images of the lesion site. Top left: Sagittal view showing mesial and distal extensions of the lesion; bottom-left: axial image showing buccal and palatal periosteal reactions; right side: coronal view showing the sun-ray appearance of a highly heterogeneous and ill-defined hyperdense lesion.

a bony hardness and non-tenderness to palpation.

Initially, a periapical radiograph was performed. The results revealed loss of lamina dura, accompanied by a radiolucent area primarily surrounding the distal aspect of the root of the maxillary right first premolar. This radiolucent area was, in turn, bordered distally by a radiopaque area within the alveolar bone. The root of the tooth was displaced mesially (Fig. 1). Root canal treatment was subsequently performed, but the swelling persisted and even increased in size over several weeks. The patient was also given antibiotics; however, no reduction in swelling was observed (Fig. 2).

Given those unsuccessful attempts to manage the lesion, the private clinic's professional decided to conduct a CBCT scan (ProMax, Planmeca, Helsinki, Finland; imaging protocol: 90 KVp, 8 mA, 12 seconds of exposure time, 0.2 mm slice thickness). This was a sectional CBCT scan, extending from the distal aspect of tooth 16 to the sagittal midline. The original Digital Imaging and Communications in Medicine (DICOM) images, along with previous 2D radiographs and patient history data, were forwarded to our department for analysis.

The CBCT images revealed a heterogeneous, hyperdense lesion with unclear boundaries located at the sites of the maxillary right canine and first premolar, causing displacement of both teeth (Figs. 3 and 4). Hyperdense images, indicative of an overextended endodontic treatment, were observed within the lesion. Alongside this, buccal and palatal periosteal reactions exhibiting a "sun-ray" appearance were detected, as well as cortical discontinuity in axial and cross-sectional views. A hypodense area, presenting a "moth-eaten" appearance consistent with bone resorption, was also discernible around the distal, mesial, and upper boundaries of the lesion. Additionally, buccal and palatal soft tissue swelling was evident around the lesion (Fig. 5). Given these findings and the short history of the lesion, the radiographic diagnosis was determined to be osteosarcoma.

Before the biopsy, a CT scan (Gemini TF 64, Philips Healthcare, Andover, MA, USA) was performed to further evaluate the lesion (Fig. 6). The scan parameters were as follows: 120 kVp tube voltage, 169 mA tube current, 1 mm slice thickness, 0.81 mm pixel spacing, and a 512 × 512 matrix. The scan revealed a mixed, ill-defined, heterogeneously hyperdense lesion in the trabecular bone of the alveolar ridge. This lesion extended vertically from the middle of the ridge to the alveolar crest, located between the maxillary right first and second premolar teeth. The buccal plate showed signs of resorption, with a hyperdense mass and lines extending beyond the boundaries of the buccal and palatal plates, indicative of periosteal proliferation. The area of soft tissue swelling was slightly larger than initially estimated with CBCT. A PET-CT scan was also conducted, covering the area from the skull vertex to the mid-thighs, with the arms raised. The scan showed no signs of adenopathy, pulmonary nodules, or other masses that could suggest potential metastasis or secondary tumors (Fig. 7).

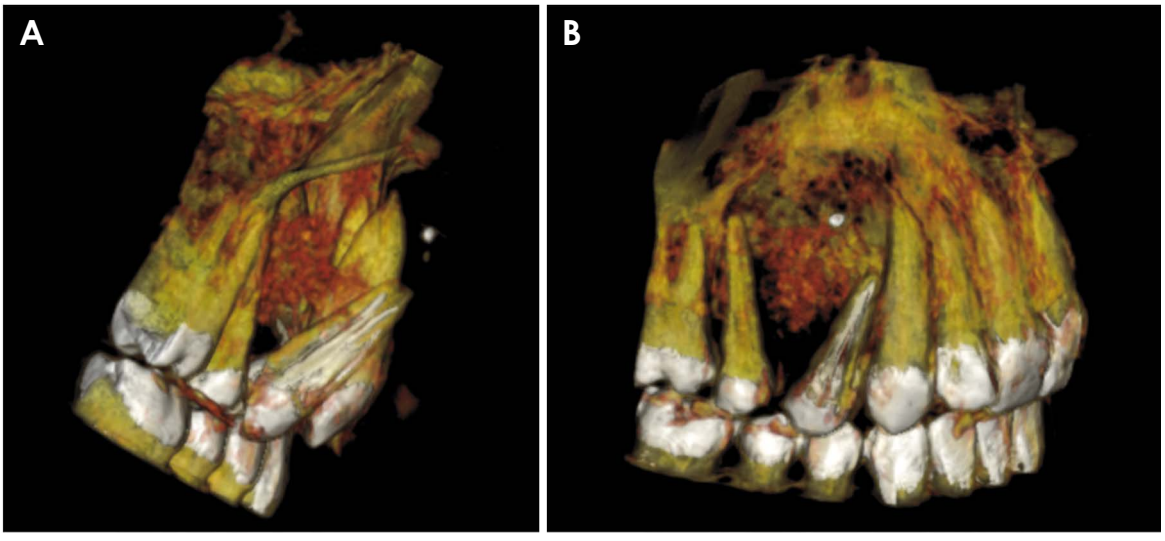

Fig. 4. Three-dimensional reconstruction of the case, augmented with threshold editing to highlight the lesion area and the displaced maxillary right first premolar (shown in both frontal and lateral views). A. A lateral view reveals the buccal displacement of the first premolar and canine in the lesion area. B. A frontal view of the lesion site displays the mesial displacement of the first premolar and the mesial-distal spread of the lesion.

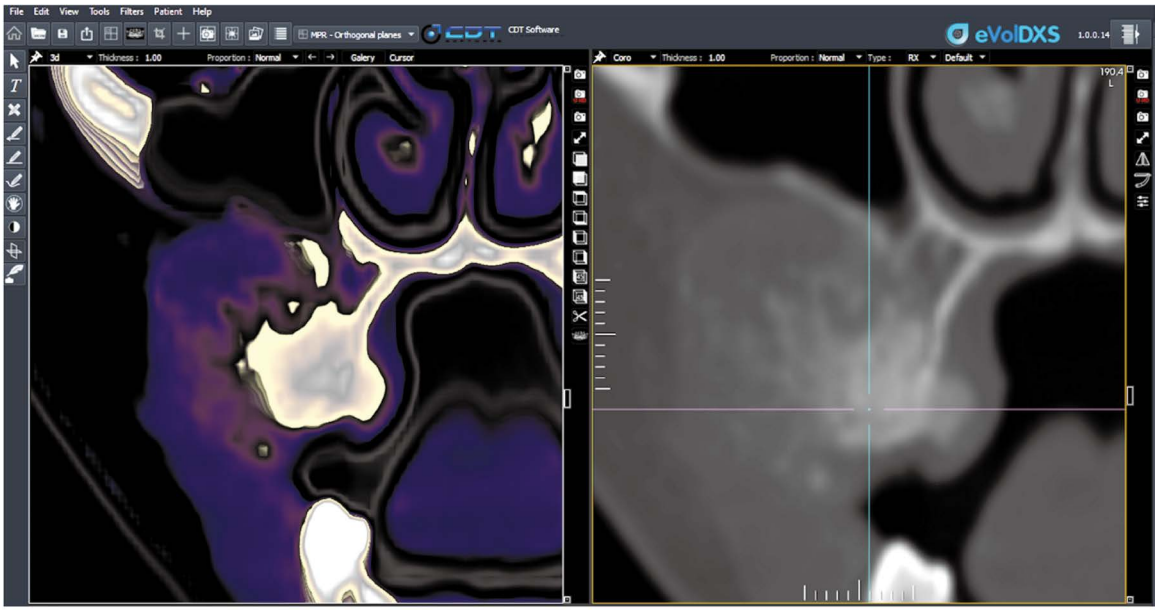

Fig. 5. Cone-beam computed tomographic filter of the eVolDXS software (CDT Software, Sao Jose dos Campos, BRAZIL). The software enhances the visualization of the lesion's extension within the soft tissues. This is demonstrated in both the 3D reconstruction (left) and the coronal image (right).

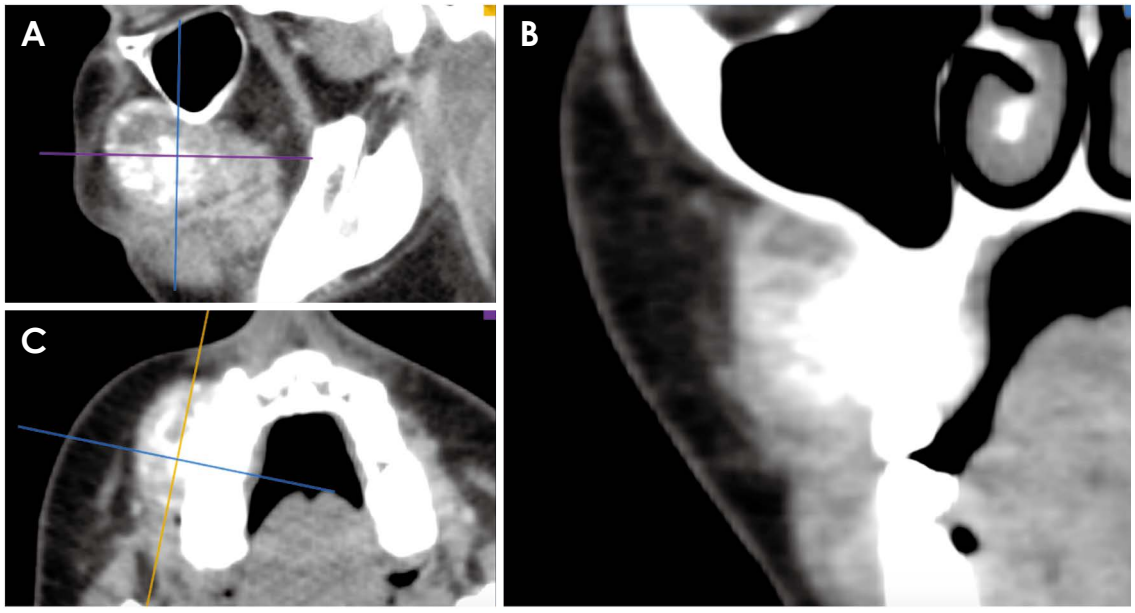

Fig. 6. A mixed, ill-defined, heterogeneous, hyperdense lesion is visible on the multi-planar reconstruction of a medical CT scan, which was imported using a DICOM viewer (Horos software, The Horos Project, Geneva, Switzerland). A. A sagittal image displays the vertical and anterior-posterior dimensions of the lesion. B. An axial image reveals the mesial-distal and buccal-palatal dimensions of the lesion, extending from the middle of the ridge to the alveolar crest between the maxillary right first and second premolar. C. A coronal image illustrates the buccal extensions of the lesion.

The patient underwent a 3-T MRI scan (Magnetom Vida, Siemens Healthcare, Erlangen, Germany) using two primary pulse sequences: a) a T1-weighted turbo spin-echo pulse sequence with a 3 mm slice thickness, 840 ms repetition time, 9.3 ms echo time, 3 averages, 3.6 mm slice gap, 401-pixel bandwidth, 127° flip angle, and a 220 × 220 field-of-view; and b) a T2-weighted spin-echo pulse sequence with a 3 mm slice thickness, 8130 ms repetition time, 103 ms echo

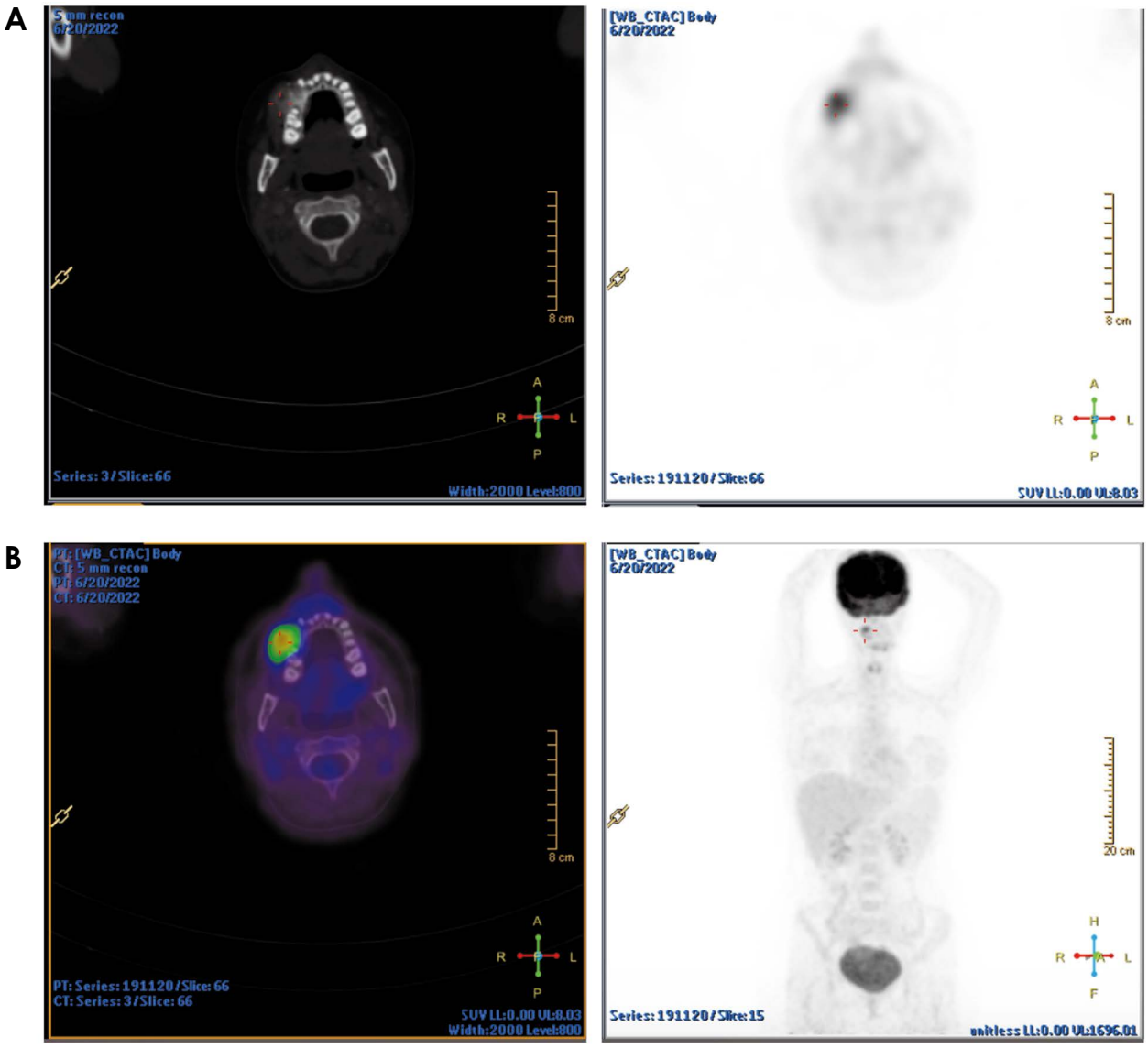

Fig. 7. PET-CT scan obtained from skull vertex to mid thighs in arms up position. A. Axial PET-CT and maximum intensity projection (MIP) images. Left: axial view shows a localized lesion in the maxillary right canine-first molar region. Right: axial positron emission tomography showing negative result. B. F-FDG (fluorodeoxyglucose) method. Left: fused axial image shows mesial-distal and buccal-palatal extensions. Right: whole-body positron emission tomography showing a negative result.

time, 1 average, 3.6 mm slice gap, 319-pixel bandwidth, 130° flip angle, and a 220 × 220 field-of-view. Both T1- and T2-weighted images showed signal inconsistency within the lesion, with the peripheral areas of the lesion displaying a lower signal than the central area near the alveolar ridge (Fig. 8). Contrast-enhanced T1-weighted images provided a clearer view of the lesion's extent, which was determined to span from the first molar to the canine sites (Fig. 9).

An incisional biopsy, consisting of a mucosal ellipse with a maximum dimension of 10 mm, revealed inflamed and ulcerated mucosa infiltrated by a malignant neoplasm. This neoplasm was composed of sheets and clusters of polygonal, spindle-shaped, and stellate cells with irregular nuclei, prominent nucleoli, and scanty amphophilic cytoplasm. Notably, there was scattered mitotic activity, with 4 mitotic figures observed per 10 high power fields. The neoplastic cells were seen to directly produce malignant osteoid, featuring central calcification and cartilaginous change. Areas of tumor necrosis were also observed. These histological characteristics were indicative of a high-grade chondroblastic osteosarcoma (Fig. 10). The patient was subsequently referred to the oncology department for neoadjuvant chemotherapy before surgical intervention, with the aim of improving prognosis and long-term survival rate. To the best

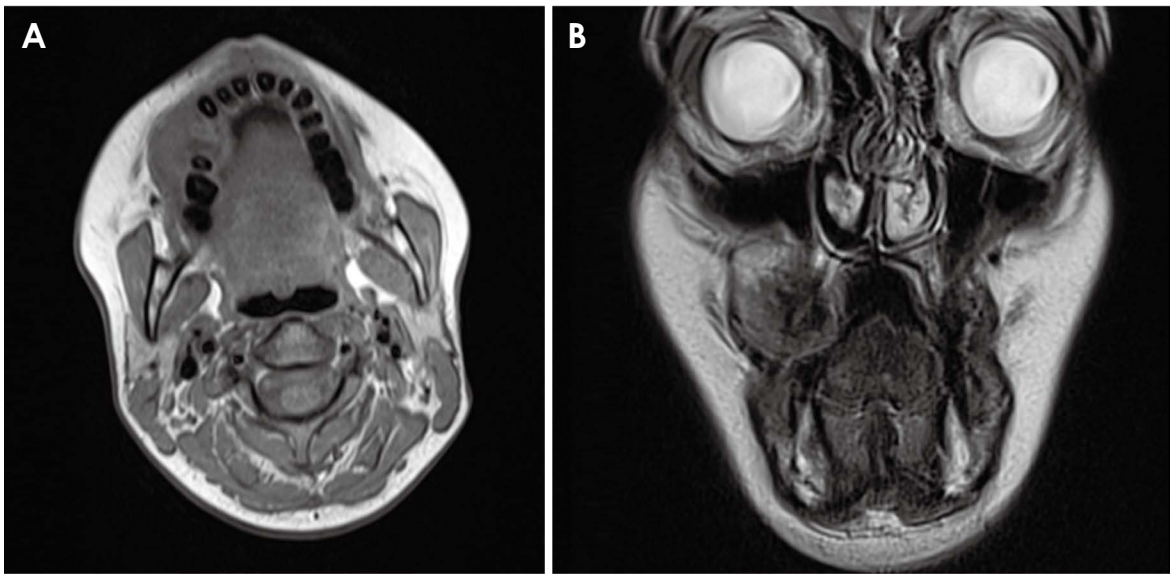

Fig. 8. A 3-T MRI scan. A. T1-weighted turbo spin-echo pulse sequence. B. T2-weighted spin-echo pulse sequence. On the left side, an axial image displays the mesial-distal and buccal-palatal extensions of the lesion, which extends from the middle of the ridge to the alveolar crest between the maxillary right canine and the first maxillary molar. On the right side, a coronal image shows the lateral-medial and vertical extensions of the lesion, which exhibit heterogeneous signal intensities.

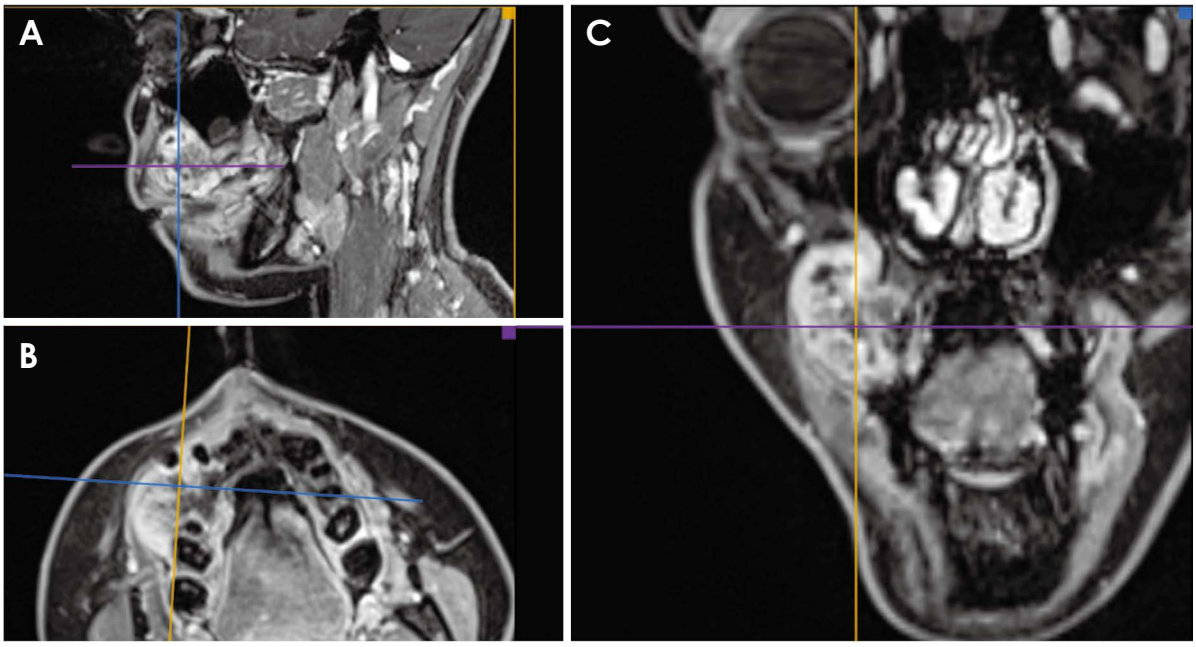

Fig. 9. A contrast-enhanced T1-weighted image reveals the extent of the lesion from the right maxillary first molar to the canine. A. A sagittal image displays the vertical and anterior-posterior dimensions of the lesion. B. An axial image illustrates the mesial-distal and buccal-palatal spread of the lesion, extending from the middle of the ridge to the alveolar crest between the right maxillary canine and the first maxillary molar. C. A coronal image presents the lateral-medial and vertical dimensions of the lesion, exhibiting heterogeneous signal intensities.

of the authors' knowledge, the patient has been following the reported treatment plan at the time of this article's publication, with no further changes in treatment or clinical presentation to date.

Discussion

This report details a rare instance of maxillary chondroblastic osteosarcoma, a diagnosis that was only possible

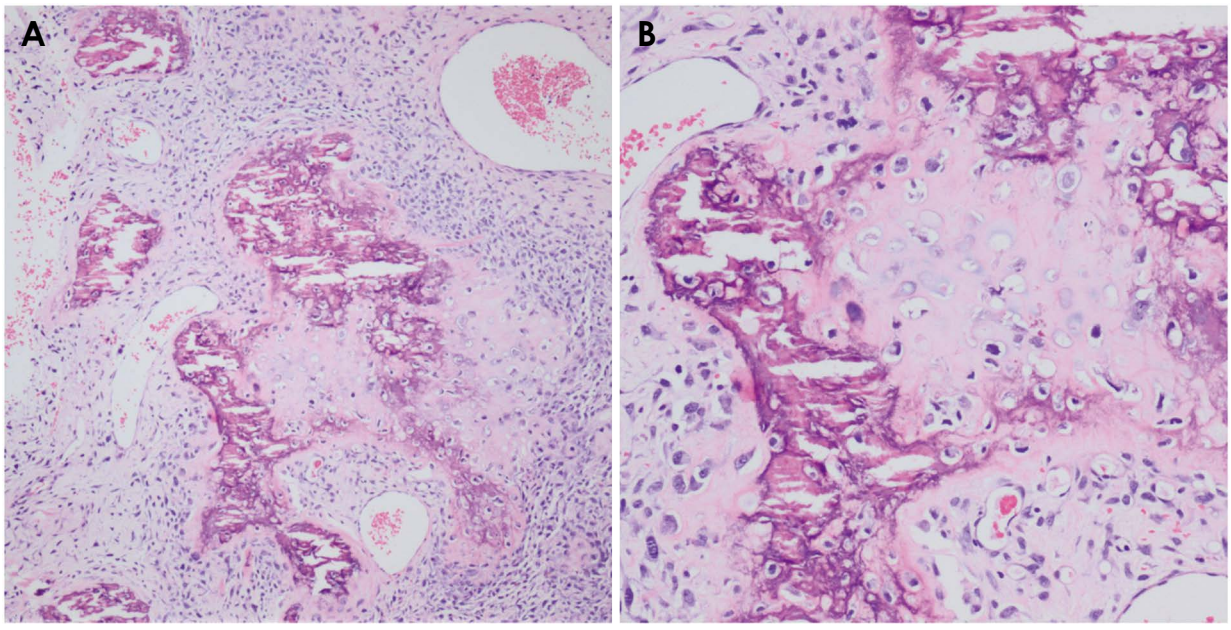

Fig. 10. A. Histopathologic examination reveals the production of malignant osteoid by pleomorphic neoplastic cells, which are polygonal, spindled, and stellate in shape (H&E stain, original magnification ×40). B. The image shows malignant osteoid undergoing central calcification and cartilaginous transformation (H&E stain, original magnification ×100).

through CBCT analysis. To confirm the diagnosis and establish a treatment plan, a CT and MRI were performed, followed by an incisional biopsy. The diagnostic process presented several challenges due to certain deviations from the typical clinical and radiographic characteristics of the lesion. Chondroblastic osteosarcoma is marked by the production of high-grade hyaline cartilage and a chondroid matrix with varying cellularity.[10] According to the literature, this pathology most frequently occurs in males between the ages of 30 and 40. However, in this case, the patient was a 17-year-old female. Another deviation is that this type of tumor is most often found in the mandible, but in this case, it developed in the premolar region of the maxilla.[7-10] The patient did not present with any pain, paresthesia, nasal obstruction, or metastasis, most likely due to the tumor's early stage. However, as with all tumors, early diagnosis is crucial for a better prognosis.[25] The patient also showed slight mobility of the affected tooth, the maxillary right first premolar. Previous research has indicated that lesions in the mandible are more likely to spread to other bones in the body (metastasize).[26,27] while lesions in the maxilla tend to affect the alveolar ridge.[28] Similar to most previously reported osteosarcomas, the lesion initially appeared as a firm, painless swelling within a period of less than 5 months.[8,10,29]

Some tumor-specific radiographic features include ill-defined margins, irregular widening of the periodontal ligament (PDL) space, and the pathognomonic sunburst or sun-ray appearance.[2,3,5] Radiographic findings can sometimes lead to misdiagnoses, with some cases being mistaken for benign fibro-osseous lesions[31] or giant cell granuloma.[28] In this particular case, initial radiolucency around the root's distal aspect led the private clinic's dentist to suspect a periapical inflammatory pathology, which prompted endodontic treatment. In retrospect, the periapical radiograph did reveal some aggressive features such as localized PDL space widening, lamina dura destruction, and ill-defined borders. However, these signs were not sufficient for a definitive diagnosis. This aligns with a previous study that found radiographic features suggestive of malignancy in 80% of the cases analyzed.[29] However, these features were not sufficient for a definitive diagnosis.

In the majority of studies, a significant delay was observed between the initial presentation and the diagnosis of tumors when 2D radiographic tools were utilized, with some cases experiencing a delay of up to 24 months.[26,30,31] However, in this particular case, a diagnosis was reached within just 3 months, thanks to the use of 3D CBCT multiplanar imaging. This technology made the lesion's characteristics more apparent when compared to the initial 2D modalities, which included either a panoramic radiograph, a standard maxillary occlusal, or a periapical radiograph. According to the guidelines published in 2015,[32] 3D CBCT is only recommended in instances where the diagnosis is uncertain, leading to an unclear treatment plan. Recent literature widely

agrees on the value of CBCT imaging in the diagnostic and treatment planning process.[33,34] A 4-year retrospective study found that the primary diagnosis and/or treatment plans were altered in 20% of cases after CBCT imaging, particularly for cases with lesions near the maxillary sinuses.[35] Weiss and Read-Fuller (2019)[34] and Schulze and Drage (2020)[36] the importance of CBCT imaging in assessing large cysts and tumors, especially when panoramic radiography alone is inadequate due to superimposition and proximity to vital structures. However, CBCT may not be sufficient for suspected malignant tumors due to its smaller contrast scale and lower soft tissue detail compared to CT, making it difficult to differentiate between cystic or solid lesions. Conversely, CBCT has been found to enhance surgeons' confidence when planning a surgical approach.[37] In this case, the "moth-eaten" and "sun-ray" appearances were only visible on the CBCT images, along with a clear understanding of all extensions, displacement of adjacent teeth, and periosteal proliferation. This led to a conclusive differential diagnosis that underscored the need for histopathology to provide a definitive diagnosis.

The patient's prognosis hinges on two primary factors: the size of the tumor and the feasibility of treatment or resection upon diagnosis.[38] In this instance, CT scans and T1- and T2-weighted MRI were utilized to verify the extent of the tumor, aligning with prior osteosarcoma studies. This held particular clinical significance for tumors in the maxillary bone, where achieving a complete tumor resection is notably challenging, leading to a higher likelihood of local recurrence compared to mandibular tumors.[38] Local recurrence is more probable than distant metastasis, with postoperative positive margins strongly linked to a poor prognosis. In terms of the patient's treatment, the current strategy of initiating chemotherapy before surgical resection is backed by existing literature.[25] Alongside chemotherapy, several studies have acknowledged the role of radiotherapy in enhancing prognosis before surgery by increasing the likelihood of achieving negative surgical margins.[10,25]

This is a single case report, so there are inherent limitations in generalizing both the clinical and radiographic presentations. It would be advisable to conduct prospective clinical studies to tackle the challenges and limitations associated with using 2D radiographic imaging modalities. Additionally, these studies could explore the utility of CBCT imaging for early tumor diagnosis in the jaws. At present, there is a scarcity of data comparing the capacity of CBCT to influence clinical outcomes and treatment planning for malignant lesions. One contributing factor to this is the limited sample size, which is due to the low prevalence of these diseases.

Within the limitations of this report, the present findings suggest that 3D imaging with CBCT is useful to make an early diagnosis of osteosarcomas in the jaws. Clinical signs and symptoms should always be evaluated in conjunction with dental radiographic findings.

Conflicts of Interest: None

References

1. Theodorou DJ, Theodorou SJ, Sartoris DJ. Primary non-odontogenic tumors of the jawbones: an overview of essential radiographic findings. Clin Imaging 2003; 27: 59-70.
2. Regezi JA, Sciubba JJ, Jordan RC. Oral pathology: clinical pathologic correlations. 6th ed. St. Louis: Elsevier/Saunders; 2012.
3. Whaites E, Drage N. Essentials of dental radiography and radiology. 5th ed. Edinburgh: Churchill Livingstone/Elsevier; 2013. p. 335.
4. Shao Z, He Y, Wang L, Hu H, Shi H. Computed tomography findings in radiation-induced osteosarcoma of the jaws. Oral Surg Oral Med Oral Pathol Oral Radiol Endod 2010; 109: e88-94.
5. Chaudhary M, Chaudhary SD. Osteosarcoma of jaws. J Oral Maxillofac Pathol 2012; 16: 233-8.
6. August M, Magennis P, Dewitt D. Osteogenic sarcoma of the jaws: factors influencing prognosis. Int J Oral Maxillofac Surg 1997; 26: 198-204.
7. Bennett JH, Thomas G, Evans AW, Speight PM. Osteosarcoma of the jaws: a 30-year retrospective review. Oral Surg Oral Med Oral Pathol Oral Radiol 2000; 90: 323-32.
8. Odel EW. Cawson's essentials of oral pathology and oral medicine. 9th ed. Edinburgh: Elsevier; 2017.
9. van Es RJ, Keus RB, van der Waal I, Koole R, Vermey A. Osteosarcoma of the jaw bones. Long-term follow up of 48 cases. Int J Oral Maxillofac Surg 1997; 26: 191-7.
10. Mamachan P, Dang V, Bharadwaj NS, DeSilva N, Kant P. Chondroblastic osteosarcoma - a case report and review of literature. Clin Case Rep 2020; 8: 2097-102.
11. Peddana SK, Ramadas R, Cherian E, Thayalan D. Chondroblastic and fibroblastic osteosarcoma of the jaws: report of two cases and review of literature. Indian J Dent Res 2017; 28: 100-4.
12. Lindqvist C, Teppo L, Sane J, Holmström T, Wolf J. Osteosarcoma of the mandible: analysis of nine cases. J Oral Maxillofac Surg 1986; 44: 759-64.
13. Anil S, Krishnan AP, Rajendran R. Osteosarcoma of the mandible masquerading as a dental abscess: report of a case. Case Rep Dent 2012; 2012: 635062.
14. Melrose RJ, Handlers JP, Kerpel S, Summerlin DJ, Tomich CJ, American Academy of Oral and Maxillofacial Pathology. The use of biopsy in dental practice. The position of the American Academy of Oral and Maxillofacial Pathology. Gen Dent 2007; 55: 457-61.
15. Ida M, Tetsumura A, Kuribayashi A, Okada N, Kurabayashi T. A clinicoradiological study of odontogenic carcinomas and their

impact on clinical diagnosis. Dentomaxillofac Radiol 2012; 41: 594-600.
16. Shumway BS, Foster TS. Pathology of the jaw: the importance of radiographs. J Can Dent Assoc 2011; 77: b132.
17. Bayrakdar IS, Yilmaz AB, Caglayan F, Ertas U, Gundogdu C, Gumussoy I. Cone beam computed tomography and ultrasonography imaging of benign intraosseous jaw lesion: a prospective radiopathological study. Clin Oral Investig 2018; 22: 1531-9.
18. De Vos W, Casselman J, Swennen GR. Cone-beam computerized tomography (CBCT) imaging of the oral and maxillofacial region: a systematic review of the literature. Int J Oral Maxillofac Surg 2009; 38: 609-25.
19. Boeddinghaus R, Whyte A. Current concepts in maxillofacial imaging. Eur J Radiol 2008; 66: 396-418.
20. Stavropoulos A, Wenzel A. Accuracy of cone beam dental CT, intraoral digital and conventional film radiography for the detection of periapical lesions. An ex vivo study in pig jaws. Clin Oral Investig 2007; 11: 101-6.
21. Yilmaz E, Kayikcioglu T, Kayipmaz S. Computer-aided diagnosis of periapical cyst and keratocystic odontogenic tumor on cone beam computed tomography. Comput Methods Programs Biomed 2017; 146: 91-100.
22. Song IS, Shin HK, Kang JH, Kim JE, Huh KH, Yi WJ, et al. Deep learning-based apical lesion segmentation from panoramic radiographs. Imaging Sci Dent 2022; 52: 351-7.
23. Poedjiastoeti W, Suebnukarn S. Application of convolutional neural network in the diagnosis of jaw tumors. Healthc Inform Res 2018; 24: 236-41.
24. Yu D, Hu J, Feng Z, Song M, Zhu H. Deep learning based diagnosis for cysts and tumors of jaw with massive healthy samples. Sci Rep 2022; 12: 1855.
25. Carrle D, Bielack SS. Current strategies of chemotherapy in osteosarcoma. Int Orthop 2006; 30: 445-51.
26. Zhao W, Cure J, Castro CY. Low-grade osteosarcoma of the jaw. Ann Diagn Pathol 2002; 6: 373-7.
27. Sinha R, Roy Chowdhury SK, Chattopadhyay PK, Rajkumar K. Low-grade osteosarcoma of the mandible. J Maxillofac Oral Surg 2010; 9: 186-90.
28. Mardinger O, Givol N, Talmi YP, Taicher S. Osteosarcoma of the jaw: the Chaim Sheba Medical Center experience. Oral Surg Oral Med Oral Pathol Oral Radiol Endod 2001; 91: 445-51.
29. Tabatabaei SH, Jahanshahi G, Dehghan Marvasti F. Diagnostic challenges of low-grade central osteosarcoma of jaw: a literature review. J Dent (Shiraz) 2015; 16: 62-7.
30. Jahanshahi G, Tabatabaie Ardakanie S. Delay in diagnosis of a low-grade osteosarcoma of mandibular symphysis; a case report. J Dent (Shiraz) 2010; 11: 177-82.
31. Diniz AF, Filho JA, Alencar Rde C, Garcia RR, Silva MR, Ribeiro-Rotta RF, et al. Low-grade central osteosarcoma of the mandible: a case study report. Oral Surg Oral Med Oral Pathol Oral Radiol Endod 2007; 103: 246-52.
32. Dula K, Bornstein MM, Buser D, Dagassan-Berndt D, Ettlin DA, Filippi A, et al. SADMFR guidelines for the use of cone-beam computed tomography/digital volume tomography. Swiss Dent J 2014; 124: 1169-83.
33. McGuigan MB, Duncan HF, Horner K. An analysis of effective dose optimization and its impact on image quality and diagnostic efficacy relating to dental cone beam computed tomography (CBCT). Swiss Den J 2018; 128: 297-316.
34. Weiss R 2nd, Read-Fuller A. Cone beam computed tomography in oral and maxillofacial surgery: an evidence-based review. Den J (Basel) 2019; 7: 52.
35. Friedlander-Barenboim S, Hamed W, Zini A, Yarom N, Abramovitz I, Chweidan H, et al. Patterns of cone-beam computed tomography (CBCT) utilization by various dental specialties: a 4-year retrospective analysis from a dental and maxillofacial specialty center. Healthcare (Basel) 2021; 9: 1042.
36. Schulze RK, Drage NA. Cone-beam computed tomography and its applications in dental and maxillofacial radiology. Clin Radiol 2020; 75: 647-57.
37. Santos AA, Yamamoto-Silva FP, Torres EM, Valladares-Neto J, Figueiredo PT, Leite AF, et al. Contribution of cone-beam computed tomography in the decision of surgical management for bone lesions of the maxillofacial region. J Craniomaxillofac Surg 2019; 47: 87-92.
38. Yildiz FR, Avci A, Dereci O, Erol B, Celasun B, Gunhan O. Gnathic osteosarcomas, experience of four institutions from Turkey. Int J Clin Exp Pathol 2014; 7: 2800-8.